Specific Adsorption of Osteopontin and Synthetic Polypeptides to Calcium Oxalate Monohydrate Crystals

Adam Taller,* Bernd Grohe,* Kem A. Rogers,† Harvey A. Goldberg,* and Graeme K. Hunter*
*Canadian Institutes of Health Research Group in Skeletal Development and Remodeling, and †Department of Anatomy and Cell Biology, Schulich School of Medicine and Dentistry, University of Western Ontario, London, Ontario, N6A 5C1, Canada

ABSTRACT Protein-crystal interactions are known to be important in biomineralization. To study the physicochemical basis of such interactions, we have developed a technique that combines confocal microscopy of crystals with fluorescence imaging of proteins. In this study, osteopontin (OPN), a protein abundant in urine, was labeled with the fluorescent dye AlexaFluor-488 and added to crystals of calcium oxalate monohydrate (COM), the major constituent of kidney stones. In five to seven optical sections along the *z* axis, scanning confocal microscopy was used to visualize COM crystals and fluorescence imaging to map OPN adsorbed to the crystals. To quantify the relative adsorption to different crystal faces, fluorescence intensity was measured around the perimeter of the crystal in several sections. Using this method, it was shown that OPN adsorbs with high specificity to the edges between {100} and {121} faces of COM and much less so to {100}, {121}, or {010} faces. By contrast, poly-L-aspartic acid adsorbs preferentially to {121} faces, whereas poly-L-glutamic acid adsorbs to all faces approximately equally. Growth of COM in the presence of rat bone OPN results in dumbbell-shaped crystals. We hypothesize that the edge-specific adsorption of OPN may be responsible for the dumbbell morphology of COM crystals found in human urine.

INTRODUCTION

Polycrystalline aggregates formed in the glomerulus or other components of the urinary system represent one of the most common forms of ectopic (extraskeletal) biomineralization. These kidney stones can contain one or more of a number of mineral phases, but the most common of these is calcium oxalate monohydrate (COM). The formation of oxalate stones is a complex process involving nucleation, growth, and aggregation of crystals in an environment containing both promoters (membranes, other crystals) and inhibitors (citrate, urinary proteins) (1).

One of the urinary proteins thought to play an important role in oxalate stone formation is osteopontin (OPN). In vitro studies have shown that OPN is a potent inhibitor of COM growth (2,3), promotes the formation of calcium oxalate dihydrate (COD) rather than monohydrate (4), and inhibits the aggregation of COM crystals (5). In vivo, OPN is the major component of the organic matrix of oxalate-containing kidney stones (6–8).

Accumulating evidence suggests that OPN is part of the body's defense mechanism against pathological calcification (9). OPN expression is upregulated in animal models of stone disease (10–14). Although mice in which the OPN gene has been inactivated exhibit no overt phenotypic abnormalities (15,16), feeding such animals a diet containing ethylene glycol results in higher levels of kidney calcification than it does in wild-type littermates (17). Based on such observations, it has been proposed that OPN acts as an inducible inhibitor of COM formation in the urinary system (18).

OPN contains ~300 amino acids, including a conserved sequence of contiguous aspartic acid residues (19). This polypeptide chain undergoes extensive posttranslational modification, including glycosylation, phosphorylation, and sulfation. The exact pattern of modification depends upon the species and tissue in which the protein is synthesized. The bovine milk isoform of OPN contains 27 sites of serine phosphorylation, 1 of threonine phosphorylation, and 3 of O-linked glycosylation (20). Human milk OPN is phosphorylated at 34 serine and 2 threonine residues, and O-glycosylated at five sites (21). The rat bone isoform has at least 29 sites of phosphorylation, 4 sites of N-linked glycosylation, and 1 site of tyrosine sulfation (22). No detailed information is available about posttranslational modification of kidney OPN. There is some disagreement in the literature about the presence of secondary structure in OPN, but it seems likely that the protein has an extended, flexible conformation (23).

Although the functional significance of posttranslational modifications in OPN is not well understood, it appears that phosphorylation is required for the inhibition of biological crystal formation. Synthetic phosphopeptides corresponding to sequences in human OPN inhibit growth and aggregation of COM crystals to a much greater degree than the nonphosphorylated counterparts (24). Phosphorylation is also required for OPN to inhibit the formation of hydroxyapatite (25–28) and calcium carbonate (29) crystals.

The aim of our research program is to determine the features of both protein and crystal that are involved in the interaction between OPN and COM. In a recent study, we used scanning confocal interference microscopy (SCIM) to measure the growth of calcium oxalate crystals in specific directions in the presence and absence of poly-L-aspartic acid (poly-asp) (30). SCIM has great potential for the study

Submitted December 1, 2006, and accepted for publication April 27, 2007.
Address reprint requests to Bernd Grohe, E-mail: bgrohe@uwo.ca.
Editor: Dagmar Ringe.

0006-3495/07/09/1768/10 $2.00
doi: 10.1529/biophysj.106.101881

of crystal growth because of its high spatial resolution, sensitivity to parallel reflecting planes such as crystal growth steps, and ability to produce time-resolved image sequences without physical contact. In this study, we combine SCIM with fluorescence imaging to visualize the adsorption of OPN and synthetic polypeptides to COM crystals. Using this approach, we demonstrate novel face- and edge-specific interactions that may be responsible for effects on the COM growth habit observed in vitro and in vivo.

MATERIALS AND METHODS

Chemicals

For precipitation of calcium oxalates, reagents used and solution preparation were as previously described (30). Poly-L-glutamic acid (poly-glu) sodium salt (~10.25 kDa) and poly-asp sodium salt (~9.15 kDa) were obtained from Sigma-Aldrich (Oakville, Canada). Alexa Fluor-488 carboxylic acid (AlexaFluor-488) was obtained from Invitrogen Canada-Molecular Probes (Burlington, Canada). Native rat bone OPN was extracted and purified as described by Goldberg and Sodek (31). The molecular weight of 37622 for OPN was determined by mass spectrometry (matrix-assisted laser desorption ionization-time of flight, Bruker Reflex III, Bruker Daltonics, Billerica, MA).

Fluorescence labeling and solution preparation of polypeptides

Poly-asp, poly-glu, and OPN were labeled with the Alexa fluorochrome according to the manufacturer's recommendations. Briefly, 5 μl of AlexaFluor-488 in dimethylformamide (10 μg/μl; high performance liquid chromatography grade, 99.9%) was added to 200 μl of polypeptide in phosphate-buffered saline (2.5 mg/ml) and 20 μl of 1 M disodium carbonate (Na_2CO_3), pH ~8.3, and incubated for 1 h at room temperature (23°C). Unconjugated label was removed by dialysis against 4 changes of 2l of Tris-buffered saline, pH 7.4, for 4 h each using 3.5-kDa dialysis tubing (Spectra/Por 3, Spectrum Laboratories, Rancho Dominquez, CA). After freeze-drying, the samples were stored at −20°C. All chemicals were supplied by Sigma-Aldrich except Na_2CO_3, which was purchased from Merck (Darmstadt, Germany). Amino acid analysis (Alberta Peptide Institute; University of Alberta, Edmonton, Canada) was carried out using norleucine as an internal standard to determine the yield of labeled peptides. The masses obtained were used to prepare aqueous stock solutions of 1 mg/ml labeled poly-asp, poly-glu, and OPN. In addition, aqueous stock solutions of 1 mg/ml and 50 μg/ml unlabeled poly-asp, poly-glu, and OPN were prepared, respectively.

Crystallization experiments

Crystallization of COM was initiated using the method previously described (30). For low supersaturation conditions (LSC), final concentrations were 1 mM calcium nitrate, 1 mM sodium oxalate, 10 mM sodium acetate, and 150 mM sodium chloride. For high supersaturation conditions (HSC), final concentrations were 2 mM calcium nitrate, 2 mM sodium oxalate, 10 mM sodium acetate, and 150 mM sodium chloride.

For scanning electron microscopy, 1-ml aliquots of these solutions were added to wells of tissue culture plates (24-well Falcon; Becton Dickinson, Franklin Lakes, NJ) containing freshly cleaved mica disks (diameter: 9.5 mm, V-1 grade, SPI Supplies, Toronto, Canada). If unlabeled poly-asp, poly-glu, or OPN was added to the wells, the volume of water was correspondingly reduced. After incubation (Ultra Tec WJ 501 S; Baxter Scientific Products, Mississauga, Canada) at 37°C for 30 min, the mica disks were rinsed with deionized water and air-dried.

Confocal microscopy was performed under LSC (see above), and 200-μl aliquots of calcium oxalate solution were added to glass-bottomed polystyrene dishes (35-mm diameter; glass bottom: grade No. 1.5, diameter: 10 mm; Mattek, Ashland, MA). Each dish was covered with laboratory film (Parafilm ''M'', Chicago, IL) to prevent evaporation and incubated at room temperature for 3 h. The dish was then placed on the heated (37°C ± 0.2°C) stage of a Zeiss LSM 410 confocal microscope (Carl Zeiss, Jena, Germany) and a 20-μl aliquot of a 1 μg/ml solution of poly-asp, poly-glu, or OPN was added to the solution. The protein or polypeptide was allowed to adsorb to the crystals for a period of 45 min before imaging. For time-course experiments, imaging started ~4 min after addition of polyelectrolytes.

The final pH of all reaction solutions was between 6.65 and 6.75; even high polyelectrolyte concentrations (up to 500 μg/ml) did not significantly change the pH.

Scanning electron microscopy

A LEO 1540XB scanning electron microscope equipped with a Gemini field emission column (Carl Zeiss, Jena, Germany) was employed. Precipitates on mica substrates were investigated without metal coating, using an acceleration voltage of 1 kV and a working distance of 3.5 mm.

Scanning confocal microscopy

SCIM (30) was used to image the crystal-glass interface. Conventional scanning confocal microscopy (SCM) was used to make optical sections at higher levels of the crystal and to image fluorescence-labeled peptides. In both cases, a 63× oil-immersion objective and a 90/10 mirror as a beam splitter were used. All procedures were carried out in the dark to avoid the effects of scattered light on crystal imaging and to prevent the fluorochrome from bleaching. Before the first scan of every crystal, prealignments of the microscope were carried out and the focus adjusted to the interface between crystal and glass. If required, the focus was adjusted again during image acquisition. Crystals were scanned using a helium/neon laser ($\lambda = 632.8$ nm). To excite the fluorochrome, a krypton/argon laser ($\lambda = 488$ nm) was used. Images of crystals were obtained in a single scan (4 s) with the gain and offset selected to provide optimal contrast of the crystal. The pinhole was adjusted to <1 airy unit to provide maximum resolution. Fluorescence images were obtained using an LP 515 emission filter (Chroma Technology, Rockingham, VT) (the emission maximum for AlexaFluor-488 is at 519 nm). Gain and offset were adjusted to provide optimal contrast, and the pinhole was set to maximum aperture. Ten large (~20 μm × 5 μm), well-formed COM crystals nucleated from a $\{010\}$ face were scanned in optical sections every 500 nm along the z axis (corresponding to the $\langle 010 \rangle$ directions of the crystal).

Image and data processing

Images were imported into Photoshop 7.0 (Adobe, San Jose, CA) and the red and green channels separated. The green-channel images were analyzed using the plot profile option in ImageJ (National Institutes of Health, Bethesda, MD). Fluorescence intensity was measured along lines corresponding to each crystal face, and the background intensity subtracted. Measurement started at the vertex between a $\{100\}$ and a $\{121\}$ face and proceeded clockwise such that the sequences of faces was (100), $(\bar{1}21)$, (121), $(\bar{1}00)$, $(12\bar{1})$, $(\bar{1}2\bar{1})$. The resulting data were transferred to Origin 5.0 (Microcal; OriginLab, Northhampton, MA) and used to plot graphs of relative fluorescence intensity (raw data minus background noise) versus fractional perimeter length (obtained by dividing actual distances by the total length of the perimeter) for each section of each crystal. Using the ''average multiple curves'' option in Origin 5.0, a mean curve for all sections of each crystal was generated. Finally, the mean curves for all 10 crystals were again averaged.

Time-course experiments

Experiments to examine polyelectrolyte adsorption with time were carried out as described in the crystallization section for confocal microscopy (see above), except that investigations started subsequently after polyelectrolytes were added to crystal-containing solutions. For image acquisition the procedure described above under ''Scanning confocal microscopy'' was modified by scanning the fluorescent profile surrounding crystals several times during a time course beginning ~4 min after polyelectrolyte addition to the crystals until the end of the elapsed time (80–100 min).

To determine the relative fluorescence intensity, green-channel images were analyzed using the plot profile option in ImageJ as described above under ''Image and data processing''. Measurements were made along lines of {100} and {121} faces and a spot representing {100}/{121} edges. The background fluorescence was then subtracted. From the measured intensities, mean values of {100}, {121}, and {100}/{121} intensities were calculated for every time segment of the time course. For the first 16 min of the time course, no above background fluorescence was detected.

RESULTS

Effects of polyelectrolytes on COM growth habit

Under LSC ($[Ca^{2+}] = [C_2O_4^{2-}] = 1$ mM), all crystals formed appear to be COM. As shown in Fig. 1, COM crystals grown on mica disks are penetration twins, with a {100} twin plane perpendicular to the ⟨100⟩ directions. The faces developed are {010}, {100}, and {121}. Most crystals nucleate from a {010} face (Fig. 1 *a*), but some nucleate from a {100} face (Fig. 1 *b*). Under HSC ($[Ca^{2+}] = [C_2O_4^{2-}] = 2$ mM), both COM and COD (not shown) morphologies are observed.

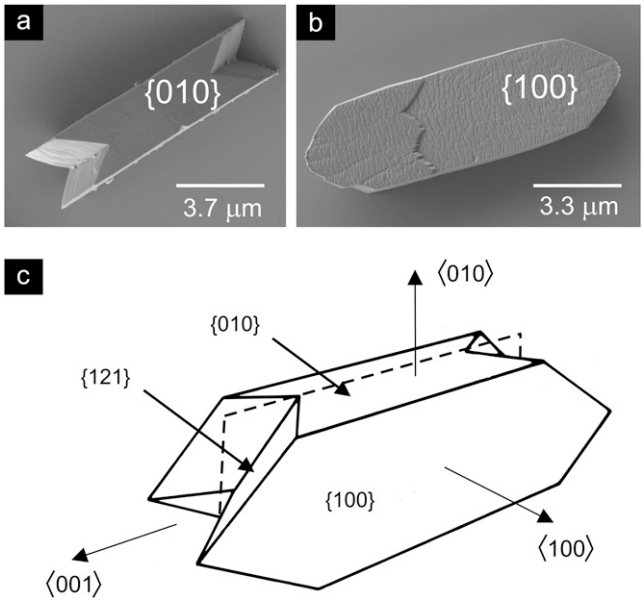

FIGURE 1 Growth habit of COM. (*a*) Scanning electron micrograph of COM crystal grown under LSC ($[Ca^{2+}] = [C_2O_4^{2-}] = 1$ mM), viewed from a ⟨010⟩ direction. (*b*) Scanning electron micrograph of COM crystal grown under LSC, viewed from a ⟨100⟩ direction. Note the presence of a macrostep on the {100} face. (*c*) Perspective view of COM penetration twin, with crystal faces developed and major crystallographic directions indicated. The dotted lines indicate the twin plane.

Using LSC, addition of OPN in the concentration range 5–10 μg/ml results in a lower number of particles formed, many of which are COD. COM crystals formed in the presence of OPN are smaller and dumbbell-shaped, lacking plane faces and interfacial angles (Fig. 2). Viewed from the ⟨100⟩ directions, these crystals are oval in cross section, with an oval-shaped depression on the {100} faces (Fig. 2 *a*); the depressions are also visible in crystals viewed from the ⟨010⟩ directions (Fig. 2 *b*). Using HSC, OPN in the range 10–15 μg/ml promotes the formation of COD but does not have an appreciable effect on overall number and size of particles. The COM crystals generated are dumbbell-shaped, with more pronounced depressions on {100} faces than those grown at low supersaturation (Fig. 2 *c*).

Under LSC, addition of poly-asp, even at concentrations as low as 1 μg/ml, induces the formation of COD (not shown). Under HSC, COM crystals formed in the presence of poly-asp (4–11 μg/ml) have some similarities to the dumbbells induced by OPN. However, the {100}-face depressions are shallower and the ratio of length (⟨001⟩ direction) to width (⟨010⟩ direction) is lower (compare Fig. 2, *c* and *d*). Another difference is that both ends of the COM crystals shown in Fig. 2 *d* exhibit a 72° angle, which is the angle formed by the {121} faces bounding the {100} faces of well-facetted COM of controls (see Fig. 1 *b*), whereas the ends of the crystals formed in the presence of OPN are rounded.

Using LSC, poly-glu, like poly-asp, results in the formation of COD, even at low polypeptide concentrations (1 μg/ml), whereas the generation of COM was rarely observed. Using HSC, addition of poly-glu (8–14 μg/ml) did not have an observable effect on overall number and size of particles, although the formation of COD crystals was promoted. COM crystals formed are roughly orthorhombic, with highly facetted faces (Fig. 2 *e*). At high magnification, these crystals exhibit features (steps and pits) containing angles characteristic of the control COM crystals (compare *inset* of Fig. 2 *e* with Fig. 1). It appears that the monohydrate phase forms superstructures organized by multiple twinning of COM both at {100} planes and along the ⟨001⟩ axis.

Adsorption of polyelectrolytes to COM

The COM crystals grown on glass-bottomed dishes under control (no additive) conditions were similar in growth habit to those grown on mica disks. These nucleated from the glass surface at either a {010} or a {100} face. For the most part, crystals nucleated from {010} were used for fluorescence imaging, as these provide better visualization of the {121} faces.

Fig. 3 shows combined SCM/fluorescence and fluorescence alone images of COM crystals to which labeled polyelectrolytes have been added. In the SCM/fluorescence images, crystals appear dark red or black and Alexa-labeled polyelectrolytes appear green. In the fluorescence alone images, Alexa-labeled polyelectrolytes appear white-gray.

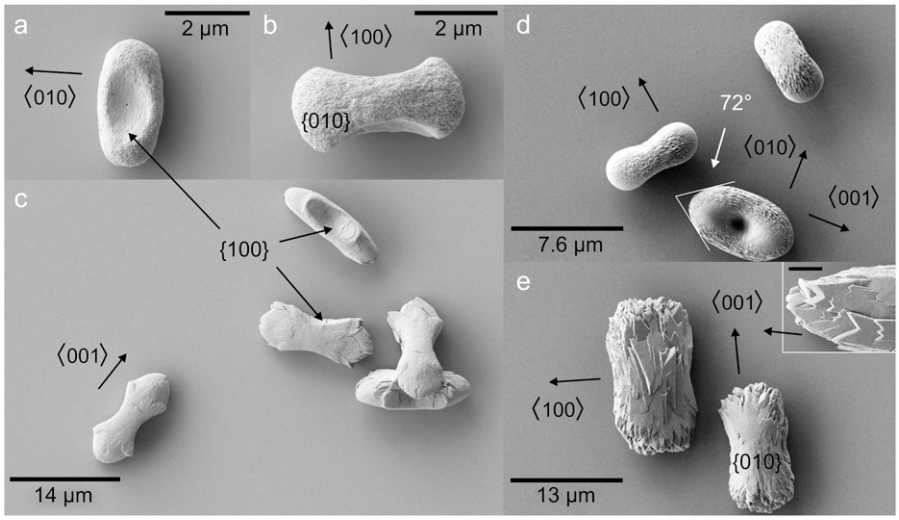

FIGURE 2 Scanning electron micrographs of COM grown in the presence of OPN, poly-asp, or poly-glu. (*a*) COM crystal grown under LSC ($[Ca^{2+}] = [C_2O_4^{2-}] = 1$ mM) in the presence of 5 μg/ml OPN. (*b*) COM crystal grown under LSC in the presence of 5 μg/ml OPN. (*c*) COM crystals grown under HSC ($[Ca^{2+}] = [C_2O_4^{2-}] = 2$ mM) in the presence of 10 μg/ml OPN. (*d*) COM crystals grown under HSC in the presence of 11 μg/ml poly-asp. E. COM crystals grown under HSC in the presence of 11 μg/ml poly-glu. (*Inset*) High-magnification image (scale bar = 3 μm) of crystal with facets similar to faces of control crystals.

As the crystals shown in Fig. 3 all nucleated from a {010} face, optical sections through them are bounded by two {100} side faces and four {121} end faces. Note that whereas the {100} faces are perpendicular to the glass surface, the {121} faces are at an oblique angle to it (see Fig. 1 *a*). For OPN, fluorescence appears to be most intense at the edges between {100} and {121} faces (Fig. 3, *a* and *b*). For poly-asp, fluorescence is concentrated along the {121} faces (Fig. 3, *c* and *d*). For poly-glu, fluorescence is approximately uniform on the {100} and {121} faces (Fig. 3, *e* and *f*).

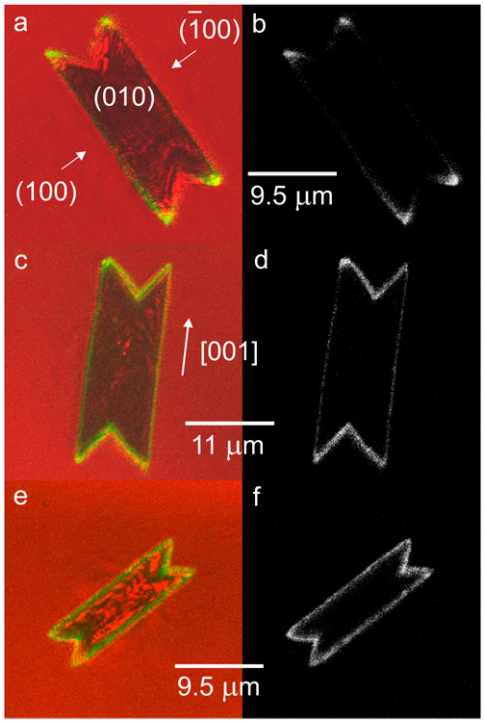

FIGURE 3 Confocal micrographs of Alexa-labeled polyelectrolytes adsorbing to COM crystals nucleated from a {010} face. (*a*, *b*) OPN. (*c*, *d*) Poly-asp. (*e*, *f*) Poly-glu. Panels *a*, *c*, and *e* are SCIM/fluorescence images of sections at the glass-crystal interface. The red (SCIM) and green (fluorescence) channels are superimposed. Panels *b*, *d*, and *f* are images using the green channel only.

As a control, SCM/fluorescence imaging was performed on COM crystals to which AlexFluor-488 alone had been added. No adsorption of the dye to COM was observed (not shown). Addition to COM of AlexaFluor-488-labeled lysozyme, a basic protein, also did not result in fluorescence significantly above background (not shown).

For OPN, poly-asp, and poly-glu, fluorescence intensity was measured around the perimeter of the crystal in several optical sections for each of 10 crystals. To account for variations in perimeter length between different sections of the same crystal and between different crystals, the length of each crystal face was divided by the total length of the perimeter. Relative intensity (RI) was then plotted against fractional perimeter distance.

Fig. 4 shows plots of RI versus fractional perimeter distance for single COM crystals labeled with OPN, poly-asp, or poly-glu. In these plots, the profiles for each section of the crystal have been superimposed. Also indicated are the points on the perimeter at which one face ends and another begins. The profiles of each optical section of a crystal are very similar. For OPN, there are four peaks of RI, corresponding to the four edges between {100} and {121} faces (Fig. 4 *a*). Between these edges, the RI falls to close to zero. For poly-asp, RI is higher (15–25 arbitrary units) along the {121} faces and lower (5–10 arbitrary units) along the {100} faces (Fig. 4 *b*). Fluorescence resulting from poly-glu adsorption is fairly uniform around the perimeter, although slightly higher at {121} faces than {100} faces (Fig. 4 *c*). Note that the RI values associated with {121} faces are similar for poly-glu and poly-asp.

Intensity profiles of the type shown in Fig. 4 were generated and averaged for each of 10 crystals labeled with

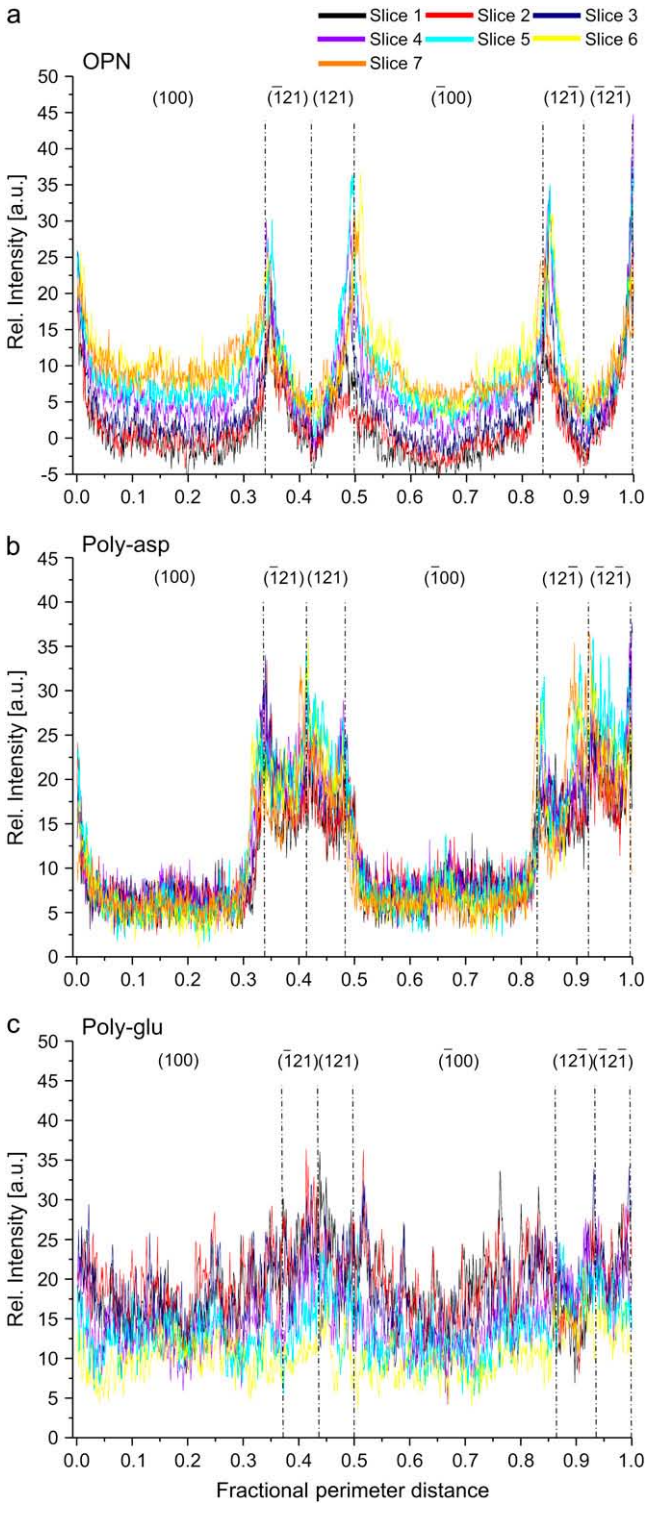

FIGURE 4 Intensity plots of polyelectrolyte fluorescence in multiple optical sections through single COM crystals. Relative fluorescence intensity, after subtraction of background, is plotted against the normalized distance around the perimeter of the crystal. The average distances occupied by the different faces present are indicated.

OPN, poly-asp, or poly-glu. The resulting profiles therefore represent the mean fluorescence intensity for all optical sections of a single crystal. The 10 profiles of each type were then superimposed (Fig. 5). Although there is some variation

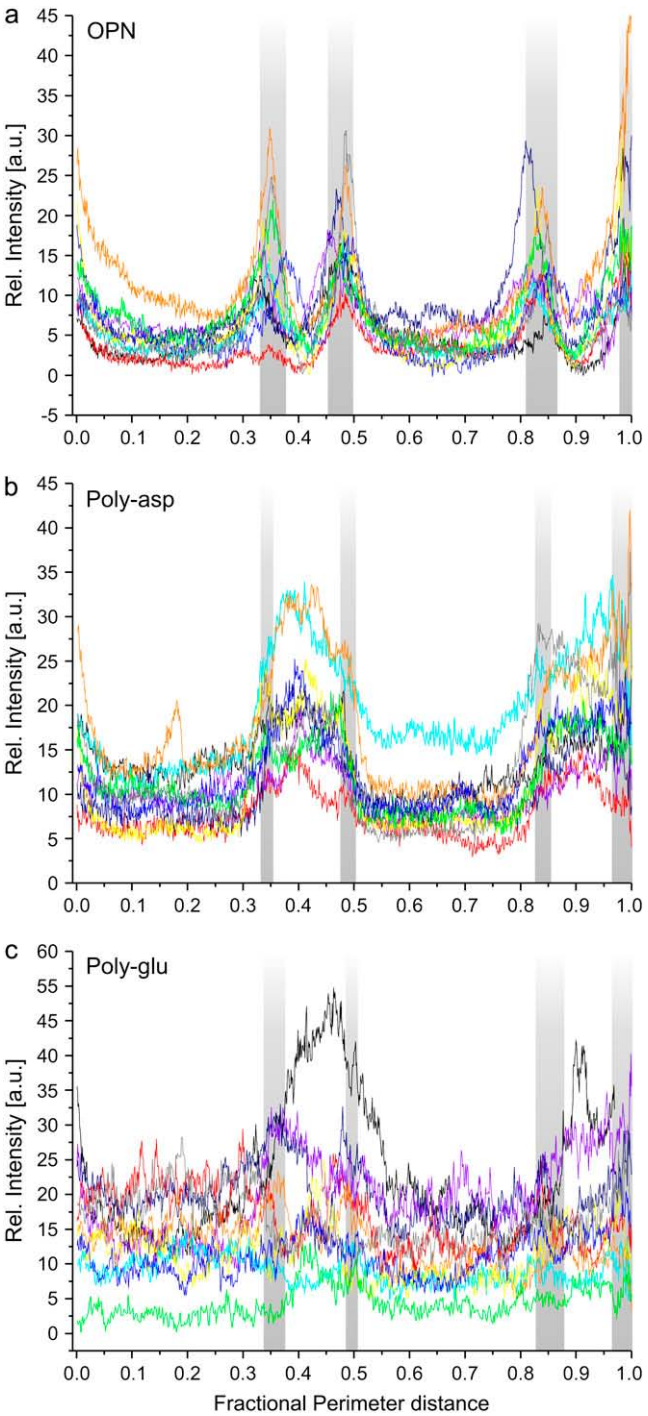

FIGURE 5 Averaged intensity plots of polyelectrolyte fluorescence in multiple COM crystals. Each plot shown represents the average intensity of multiple optical sections through a single COM crystal. The gray bars represent the range of fractional perimeter distance values for the edges between {100} and {121} faces.

(for example, *orange line* for poly-asp, *black line* for poly-glu), in general the profiles are very similar.

The 10 profiles shown in Fig. 5 were then averaged, and the resulting profiles are shown in Fig. 6. These plots represent the average of all sections for all 10 crystals. From these profiles it appears that OPN adsorption is strongly associated with the {100}/{121} edges (Fig. 6 *a*); poly-asp is strongly associated with {121} faces (Fig. 6 *b*); and poly-glu is significant at all faces, although perhaps higher at {121} faces (Fig. 6 *c*).

Because the {121} faces of COM crystals nucleated from a {010} face are not parallel to the microscopic *z* axis (see Fig. 1 *a*), the area of a {121} face included within an optical section will be higher than the area of a {100} face. This factor probably accounts for the slightly higher fluorescence intensity associated with {121} faces of COM labeled with poly-glu (Fig. 6 *c*) but is not sufficient to explain the intensity of poly-asp on those faces.

The images and data in Figs. 3–6 were all obtained from crystals nucleated from a {010} face. Panels *a–d* of Fig. 7 show two crystals, one nucleated from {010} and the other from {100}, labeled with poly-asp. Panels *a* and *b* are composite (*red-green*) images taken at the glass-crystal interface and at the crystal-solution interface of the latter crystal, respectively. Panels *c* and *d* are green-channel (fluorescence) images corresponding to panels *a* and *b*, respectively. From the glass-crystal sections (*a* and *c*), poly-asp binding to the {121} faces can be seen in both crystals. From the crystal-solution sections (*b* and *d*), it is clear that there is negligible binding to the {100} face. Panels *e* and *f* of Fig. 7 are images of crystals nucleated from a {100} face and labeled with poly-glu and OPN, respectively. Poly-glu adsorption occurs on {010} (side) and {121} (end) faces, although slightly more on the latter. As noted above, this is likely to be because the {121} faces are not vertical. OPN adsorption is seen at the {121}/{100} edges, as it was for crystals nucleated from {010} faces (Fig. 3 *a*).

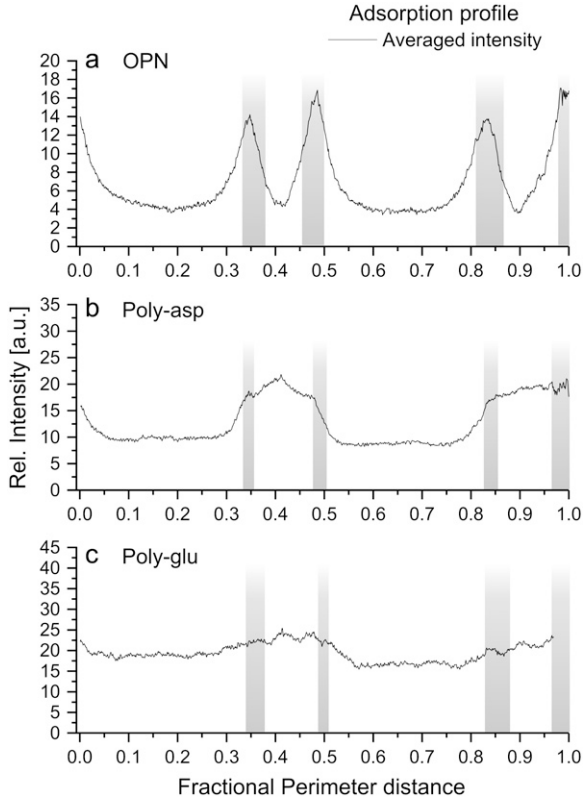

FIGURE 6 Averaged intensity plots of polyelectrolyte fluorescence in multiple sections of multiple COM crystals. These plots were generated by averaging the data shown in Fig. 5. The gray bars represent the range of fractional perimeter distance values for the edges between {100} and {121} faces.

Kinetics of OPN adsorption to COM

To determine the rate of adsorption of OPN to COM, AlexaFluor-488-labeled protein was added to crystal-containing solutions prepared as described above and fluorescence associated with {100} and {121} faces and {100}/{121} edges quantified approximately every 4 min for a total of 90 min. Representative data are shown in Fig. 8. No above background fluorescence was observed for the first 16 min, presumably because the amount of Alexa-labeled protein adsorbed was below the detection threshold of the camera. Thereafter, fluorescence intensity increased in a sigmoid fashion, reaching a plateau after ~60 min. The final amounts of fluorescence associated with {100}/{121} edges (B_{max} = 5.26) was ~100% higher than those associated with the {100} (B_{max} = 2.66) and {121} (B_{max} = 2.25) faces.

DISCUSSION

Effects of polyelectrolytes on COM growth habit

Although it is well established that OPN inhibits the growth of COM, the effect of the protein on crystal growth habit have not been previously reported. We show here that COM crystals grown in the presence of OPN are morphologically quite different from the prismatic penetration twins formed in the absence of the protein. Within the concentration range used, OPN induces the formation of dumbbell-shaped crystals with roughened surfaces and rounded edges. To test the specificity of this effect, COM was also grown in the presence of the synthetic polypeptides poly-asp and poly-glu. Because aspartic acid- and glutamic acid-rich sequences have been implicated in the interactions of OPN and other mineral-binding proteins with COM and other mineral phases (24,32), the effects of poly-asp and poly-glu on crystal formation are often studied (33–35). Crystals grown with poly-asp are generally similar in growth habit to those grown with OPN, particularly in that both show depressions on the surfaces that we believe to be the {100} faces. Poly-glu also has profound effects on the growth habit of COM. However,

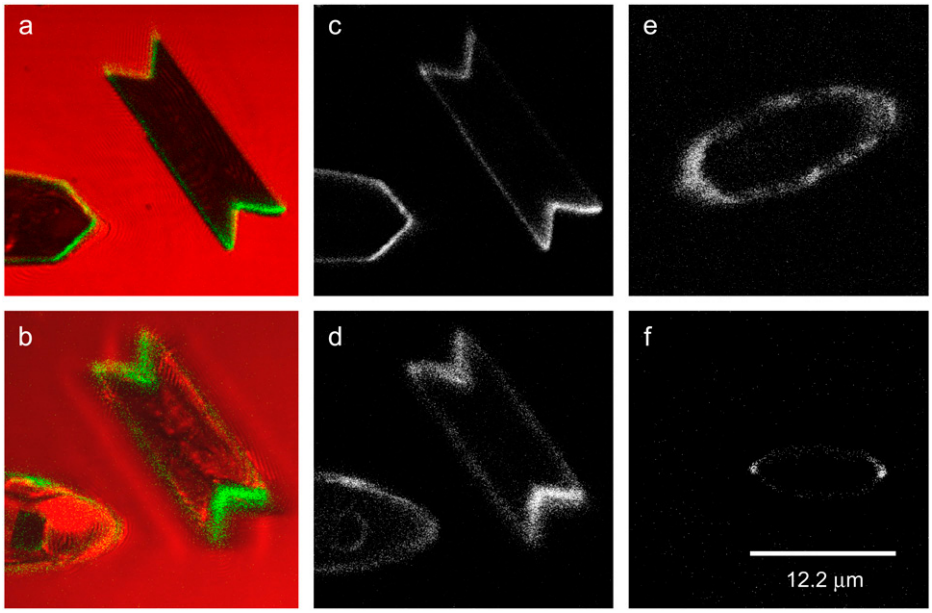

FIGURE 7 Confocal micrographs of Alexa-labeled polyelectrolytes adsorbing to COM crystals nucleated from {100} and {010} faces. (*a–d*) Poly-asp. The crystals at upper right and lower left were nucleated from {010} and {100} faces, respectively. (*a*) SCIM/fluorescence image of poly-asp adsorption at the crystal-glass interface. (*b*) SCM/fluorescence image of poly-asp adsorption at the crystal-solution interface of the crystal shown in lower left. (*c*) Fluorescence image of section shown in *a*. (*d*) Fluorescence image of section shown in *b*. (*e*) SCM/fluorescence image of poly-glu adsorption to COM crystal nucleated from a {100} face. (*f*) SCM/fluorescence image of OPN adsorption to COM crystal nucleated from a {100} face.

crystals grown with poly-glu generally lack the rounded edges and regularity of those grown with OPN or poly-asp.

In previous studies, Wesson and co-workers found that growth of COM in the presence of poly-glu resulted in smaller, dumbbell-like crystals (33). The term ''dumbbell'' was also applied to COM crystals grown in the presence of heparin (36). In the latter study, the indexing of the crystals agrees with our identification of the concave faces as {100}. It is apparent that the effects of polyanions on COM growth habit are highly dependent upon the experimental conditions used. However, the striking similarities between our OPN-induced dumbbells and the COM crystals found in human crystalluria (37) and in the urine of individuals suffering from intoxication with ethylene glycol, a metabolic precursor of oxalate (38), suggest that modification of the COM growth habit is a physiological effect of OPN in urine.

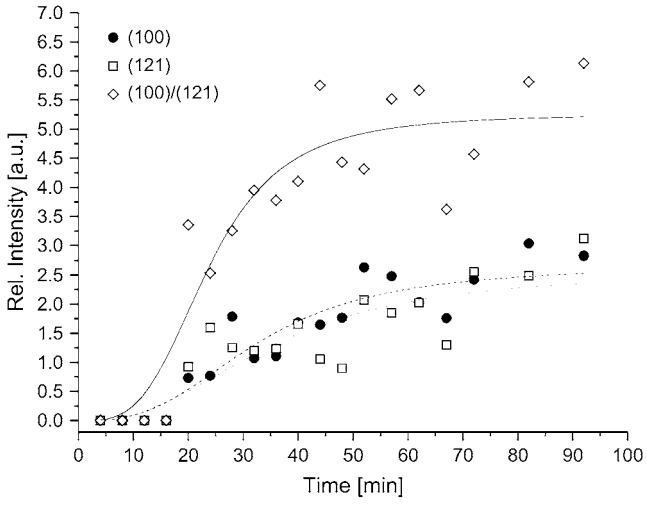

FIGURE 8 Kinetics of OPN adsorption to COM crystals. Sigmoid binding curves were fitted to the data points using Origin.

Specificity of synthetic polypeptide adsorption to COM

The interaction between synthetic polypeptides and COM was studied in multiple optical sections through crystals using a combination of SCM and fluorescence imaging. By quantifying the fluorescence associated with different faces and interfacial edges, we have shown that poly-asp adsorbs preferentially to {121} faces and poly-glu adsorbs nonspecifically to {100}, {010}, and {121} faces.

Previous studies on interactions between polyelectrolytes and COM crystals have mainly used in situ atomic force microscopy (AFM). In these studies, rates of movement of steps on crystal surfaces (or rates of filling of etch pits, which is essentially the same thing) are used to infer the site of binding of inhibitors. The rational is that binding to a particular crystal face will inhibit growth perpendicular to that face; that is, a substance adsorbing to {*hkl*} faces will inhibit growth in ⟨*hkl*⟩ directions (39).

AFM analysis of COM growth showed that poly-glu was more potent than poly-asp in inhibiting the movement of growth hillocks on {010} faces in both the ⟨021⟩ and ⟨121⟩ directions; however, poly-asp was more potent than poly-glu in inhibiting the movement of hillocks on {100} faces in ⟨001⟩ directions (35). These inhibitory effects were attributed to ''pinning'' of the steps formed by the edges of the hillock and the underlying crystal face.

Studies on the filling of etch pits on {100} faces of COM indicated that poly-asp interacts preferentially with {001} or

{021} lattice planes, whereas poly-glu prefers {010} planes (34). A recent study using AFM has confirmed that aspartic acid-rich peptides inhibit growth of hillocks on {100} faces in ⟨001⟩ directions more effectively than in ⟨021⟩ directions (40). It is interesting that peptides of sequence $(asp\text{-}asp\text{-}asp\text{-}ser)_n$ were much better inhibitors than those of sequence $(asp\text{-}asp\text{-}asp\text{-}gly)_n$, as OPN contains numerous sequences rich in both aspartic acid and serine.

As noted by Jung et al., pinning of a particular step could be caused by interactions with different lattice planes. For example, the poly-asp-mediated inhibition of step growth in the ⟨001⟩ direction on the (100) face of COM could result from the polypeptide adsorption to either the (001) face of the step, the (100) face itself, or both. These possibilities can be distinguished by studying the effects of inhibitors on the overall growth of the crystal. Using real-time SCIM imaging, we determined growth rates of COM crystals nucleated from {100} faces. It was found that poly-asp decreased growth in ⟨001⟩ directions but not in ⟨010⟩ directions (30). Because COM crystals of the growth habit studied will grow in ⟨001⟩ directions only by lattice-ion addition to {121} faces, adsorption of poly-asp to these faces would be expected to inhibit growth along ⟨001⟩ (see Fig. 1 *c*). Therefore, the face-specific adsorption of poly-asp to COM observed in this study is generally consistent with previous studies on the effects of poly-asp on crystal growth.

In the case of poly-glu, the pattern of adsorption to COM crystals and effects on growth habit are more difficult to correlate. Real-time SCIM analysis may be of value in determining whether poly-glu inhibits growth in all directions equally, as predicted by this study, or unequally, as suggested by the AFM studies cited above.

Specificity of OPN adsorption to COM

In a previous study, fluorescence microscopy was used to study the interaction between rhodamine-labeled staphylococcal protein A and COM crystals. It was shown that protein adsorbs to {110} planes and is incorporated into the crystal lattice (41). In this study, we use a similar technique to show that OPN adsorbs preferentially to the edges between {100} and {121} faces of COM crystals.

In situ AFM analysis by Qiu et al. (42) showed that human kidney OPN strongly inhibits movement of growth hillocks on {010} faces of COM, which grow in the ⟨101⟩ and ⟨100⟩ directions. (In the indexing scheme used by Qiu et al., ⟨101⟩ and ⟨100⟩ directions are equivalent to the ⟨100⟩ and ⟨001⟩ directions used here.) However, OPN had minimal effect on growth hillocks on {101} faces, which grow in ⟨120⟩ and ⟨100⟩ directions (equivalent to ⟨021⟩ and ⟨001⟩ directions in the indexing scheme used here). The different effects of OPN on growth of the {010} and {101} faces were attributed to the greater height of hillocks on the former, rather than face-specific binding of the protein.

Using a different AFM technique, the strength of interaction of carboxylate- or amidinium-functionalized tips with faces of COM crystals was shown to be {100} > {121} > {010}. Addition of bovine milk OPN resulted in an increased adhesion of the tips to {100} faces, suggesting that the protein is preferentially adsorbing to these faces (43).

If OPN preferentially adsorbs to {010} faces of COM, it should decrease growth of the crystals in ⟨010⟩ directions; if it preferentially adsorbs to {100} faces, OPN should decrease growth in ⟨100⟩ directions. In fact, as we have shown, the effects of OPN on COM growth habit are more complex than can be explained solely by inhibition of growth in a specific set of directions. We have also shown that the greatest degree of adsorption of OPN to COM is not associated with a particular face but with the edges between {100} and {121} faces. We hypothesize that this edge-specific binding is responsible for the dumbbell morphology of COM crystals grown in the presence of OPN and, indeed, COM crystals found in human urine.

The mechanism by which OPN adsorbs to {100}/{121} edges of COM is not immediately obvious. One possible explanation is that OPN is actually interacting with {021} faces lying between {100} and {121}. Such faces have been reported to develop in COM penetration twins (44) and are occasionally observed under the conditions used in this study, particularly at longer incubation times (>3.5 h). COM crystals with well-developed {021} faces have an overall shape similar to dumbbell crystals (compare Fig. 6 of Millan (44) with Fig. 2 *c* of this work). However, {021} crystals of COM would be expected to exhibit interfacial edges.

Another possibility is that these edges are sites of high surface energy (45). The acute angles formed by the {100} and {121} faces would support this possibility. Adsorption of OPN at edges rather than faces might well be related to the loss of edges in COM dumbbells.

CONCLUSION

A combination of confocal microscopy and fluorescence imaging has been used to directly demonstrate that OPN adsorbs preferentially to {100}/{121} edges of preformed COM crystals. We propose that this edge-specific interaction is responsible for the dumbbell morphology observed in COM crystals grown in the presence of OPN and also in human crystalluria. The confocal/fluorescence imaging technique described here can be used to study a wide variety of protein-crystal interactions, including those relevant to biomineralization and biomimetic material design.

We thank Silvia Mittler, Department of Physics and Astronomy, University of Western Ontario, for many helpful discussions. The expert technical assistance of Honghong Chen and Kari Ann Orlay is gratefully acknowledged. Mira Rasch made the drawing shown in Fig. 1 *c*.

The studies reported here were supported by the Canadian Institutes of Health Research.

REFERENCES

1. Lieske, J. C., and F. G. Toback. 2000. Renal cell-urinary crystal interactions. *Curr. Opin. Nephrol. Hypertens.* 9:349–355.
2. Shiraga, H., W. Min, W. J. VanDusen, M. D. Clayman, D. Miner, C. H. Terrell, J. R. Sherbotie, J. W. Foreman, C. Przysiecki, E. G. Nielson, and J. R. Hoyer. 1992. Inhibition of calcium oxalate crystal growth *in vitro* by uropontin: another member of the aspartic acid-rich protein superfamily. *Proc. Natl. Acad. Sci. USA.* 89:426–430.
3. Worcester, E. M., S. S. Blumenthal, A. M. Beshensky, and D. L. Lewand. 1992. The calcium oxalate crystal growth inhibitor protein produced by mouse kidney cortical cells in culture is osteopontin. *J. Bone Miner. Res.* 7:1029–1036.
4. Wesson, J. A., E. M. Worcester, J. H. Wiessner, N. S. Mandel, and J. G. Kleinman. 1998. Control of calcium oxalate crystal structure and cell adherence by urinary macromolecules. *Kidney Int* 53:952–957.
5. Wesson, J. A., V. Ganne, A. M. Beshensky, and J. G. Kleinman. 2005. Regulation by macromolecules of calcium oxalate crystal aggregation in stone formers. *Urol. Res.* 33:206–212.
6. Hoyer, J. R. 1994. Uropontin in urinary calcium stone formation. *Miner. Electrolyte Metab.* 20:385–392.
7. Atmani, F., P. A. Glenton, and S. R. Khan. 1998. Identification of proteins extracted from calcium oxalate and calcium phosphate crystals induced in the urine of healthy and stone forming subjects. *Urol. Res.* 26:201–207.
8. McKee, M. D., A. Nanci, and S. R. Khan. 1995. Ultrastructural immunodetection of osteopontin and osteocalcin as major matrix components of renal calculi. *J. Bone Miner. Res.* 10:1913–1929.
9. Kleinman, J. G., J. A. Wesson, and J. Hughes. 2004. Osteopontin and calcium stone disease. *Nephron Physiol.* 98:43–47.
10. Gokhale, J. A., P. A. Glenton, and S. R. Khan. 1996. Localization of Tamm-Horsfall protein and osteopontin in a rat nephrolithiasis model. *Nephron.* 73:456–461.
11. Yagisawa, T., P. S. Chandhoke, J. Fan, and S. Lucia. 1998. Renal osteopontin expression in experimental urolithiasis. *J. Endourol.* 12:171–176.
12. Kohri, K., S. Nomura, Y. Kitamura, T. Nagata, K. Yoshioka, M. Iguchi, T. Yamate, T. Umekawa, Y. Suzuki, H. Sinohara, and T. Kurita. 1993. Structure and expression of the mRNA encoding urinary stone protein (osteopontin). *J. Biol. Chem.* 268:15180–15184.
13. Yasui, T., K. Fujita, S. Sasaki, M. Sato, M. Sugimoto, S. Hirota, Y. Kitamura, S. Nomura, and K. Kohri. 1999. Expression of bone matrix proteins in urolithiasis model rats. *Urol. Res.* 27:255–261.
14. Jiang, X. J., T. Feng, L. S. Chang, X. T. Kong, G. Wang, Z. W. Zhang, and Y. L. Guo. 1998. Expression of osteopontin mRNA in normal and stone-forming rat kidney. *Urol. Res.* 26:389–394.
15. Liaw, L., D. E. Birk, C. B. Ballas, J. S. Whitsitt, J. M. Davidson, and B. L. M. Hogan. 1998. Altered wound healing in mice lacking a functional osteopontin gene (spp1). *J. Clin. Invest.* 101:1468–1478.
16. Rittling, S. R., H. N. Matsumoto, M. D. McKee, A. Nanci, X. R. An, K. E. Novick, A. J. Kowalski, M. Noda, and D. T. Denhardt. 1998. Mice lacking osteopontin show normal development and bone structure but display altered osteoclast formation in vitro. *J. Bone Miner. Res.* 13:1101–1111.
17. Wesson, J. A., R. J. Johnson, M. Mazzali, A. M. Beshensky, S. Stietz, C. Giachelli, L. Liaw, C. E. Alpers, W. G. Couser, J. G. Kleinman, and J. Hughes. 2003. Osteopontin is a critical inhibitor of calcium oxalate crystal formation and retention in renal tubules. *J. Am. Soc. Nephrol.* 14:139–147.
18. Mo, L., H. Y. Huang, X. H. Zhu, E. Shapiro, D. L. Hasty, and X. R. Wu. 2004. Tamm-Horsfall protein is a critical renal defense factor protecting against calcium oxalate crystal formation. *Kidney Int.* 66: 1159–1166.
19. Sodek, J., B. Ganss, and M. D. McKee. 2000. Osteopontin. *Crit. Rev. Oral Biol. Med.* 11:279–303.
20. Sørensen, E. S., P. Højrup, and T. E. Petersen. 1995. Posttranslational modifications of bovine osteopontin: identification of twenty-eight phosphorylation and three O-glycosylation sites. *Protein Sci.* 4:2040–2049.
21. Christensen, B., M. S. Nielsen, K. F. Haselmann, T. E. Petersen, and E. S. Sorensen. 2005. Post-translationally modified residues of native human osteopontin are located in clusters: identification of 36 phosphorylation and five O-glycosylation sites and their biological implications. *Biochem. J.* 390:285–292.
22. Keykhosravani, M., A. Doherty-Kirby, C. Zhang, D. Brewer, H. A. Goldberg, G. K. Hunter, and G. Lajoie. 2005. Comprehensive identification of post-translational modifications of rat bone osteopontin by mass spectrometry. *Biochemistry.* 44:6990–7003.
23. Fisher, L. W., D. A. Torchia, B. Fohr, M. F. Young, and N. S. Fedarko. 2001. Flexible structures of SIBLING proteins, bone sialoprotein and osteopontin. *Biochem. Biophys. Res. Commun.* 280:460–465.
24. Hoyer, J. R., J. R. Asplin, and L. Otvos. 2001. Phosphorylated osteopontin peptides suppress crystallization by inhibiting the growth of calcium oxalate crystals. *Kidney Int.* 60:77–82.
25. Boskey, A. L., M. Maresca, W. Ullrich, S. B. Doty, W. T. Butler, and C. W. Prince. 1993. Osteopontin-hydroxyapatite interactions in vitro. Inhibition of hydroxyapatite formation and growth in a gelatin-gel. *Bone Miner.* 22:147–159.
26. Hunter, G. K., C. L. Kyle, and H. A. Goldberg. 1994. Modulation of crystal formation by bone phosphoproteins: structural specificity of the osteopontin-mediated inhibition of hydroxyapatite formation. *Biochem. J.* 300:723–728.
27. Pampena, D. A., K. A. Robertson, O. Litvinova, G. Lajoie, H. A. Goldberg, and G. K. Hunter. 2004. Inhibition of hydroxyapatite formation by osteopontin phosphopeptides. *Biochem. J.* 378:1083–1087.
28. Jono, S., C. Peinado, and C. M. Giachelli. 2000. Phosphorylation of osteopontin is required for inhibition of vascular smooth muscle cell calcification. *J. Biol. Chem.* 275:20197–20203.
29. Hincke, M. T., and M. St. Maurice. 2000. Chapter 3. *In* Chemistry and Biology of Mineralized Tissues: Proceedings of the Sixth International Conference, Vittel, France, 1998. M. Goldberg, A. Boskey, and C. Robinson, editors. American Academy of Orthopaedic Surgeons, Rosemont, IL. 13–17.
30. Grohe, W., K. Rogers, H. A. Goldberg, and G. K. Hunter. 2006. Crystallization kinetics of calcium oxalate hydrates studied by scanning confocal interference microscopy. *J. Cryst. Growth.* 295:148–157.
31. Goldberg, H. A., and J. Sodek. 1994. Purification of mineralized tissue-associated osteopontin. *J. Tissue Cult. Methods.* 16:211–215.
32. Goldberg, H. A., K. J. Warner, M. C. Li, and G. K. Hunter. 2001. Binding of bone sialoprotein, osteopontin and synthetic polypeptides to hydroxyapatite. *Connect. Tissue Res.* 42:25–37.
33. Wesson, J. A., E. M. Worcester, and J. G. Kleinman. 2000. Role of anionic proteins in kidney stone formation: interaction between model anionic polypeptides and calcium oxalate crystals. *J. Urol.* 163:1343–1348.
34. Guo, S. W., M. D. Ward, and J. A. Wesson. 2002. Direct visualization of calcium oxalate monohydrate crystallization and dissolution with atomic force microscopy and the role of polymeric additives. *Langmuir.* 18:4284–4291.
35. Jung, T., X. Sheng, C. K. Choi, W. S. Kim, J. A. Wesson, and M. D. Ward. 2004. Probing crystallization of calcium oxalate monohydrate and the role of macromolecule additives with in situ atomic force microscopy. *Langmuir.* 20:8587–8596.
36. Shirane, Y., Y. Kurokawa, Y. Sumiyoshi, and S. Kagawa. 1995. Morphological effects of glycosaminoglycans on calcium oxalate monohydrate crystals. *Scanning Microsc.* 9:1081–1088 (discussion 1088).
37. Bader, C. A., A. Chevalier, C. Hennequin, P. Jungers, and M. Daudon. 1994. Methodological aspects of spontaneous crystalluria studies in calcium stone formers. *Scanning Microsc.* 8:215–232.
38. Morfin, J., and A. Chin. 2005. Images in clinical medicine. Urinary calcium oxalate crystals in ethylene glycol intoxication. *N. Engl. J. Med.* 353:e21.

39. Addadi, L., and S. Weiner. 1985. Interactions between acidic proteins and crystals: stereochemical requirements in biomineralization. *Proc. Natl. Acad. Sci. USA.* 82:4110–4114.

40. Wang, L., S. R. Qiu, W. Zachowicz, X. Guan, J. J. DeYoreo, G. H. Nancollas, and J. R. Hoyer. 2006. Modulation of calcium oxalate crystallization by linear aspartic acid-rich peptides. *Langmuir.* 22: 7279–7285.

41. Touryan, L. A., R. H. Clark, R. W. Gurney, P. S. Stayton, B. Kahr, and V. Vogel. 2001. Incorporation of fluorescent molecules and proteins into calcium oxalate monohydrate single. *J. Cryst. Growth.* 233: 380–388.

42. Qiu, S. R., A. Wierzbicki, C. A. Orme, A. M. Cody, J. R. Hoyer, G. H. Nancollas, S. Zepeda, and J. J. DeYoreo. 2004. Molecular modulation of calcium oxalate crystallization by osteopontin and citrate. *Proc. Natl. Acad. Sci. USA.* 101:1811–1815.

43. Sheng, X., T. Jung, J. A. Wesson, and M. D. Ward. 2005. Adhesion at calcium oxalate crystal surfaces and the effect of urinary constituents. *Proc. Natl. Acad. Sci. USA.* 102:267–272.

44. Millan, A. 2001. Crystal growth shape of whewellite polymorphs: influence of structure distortions on crystal shape. *Cryst. Growth Des.* 1:245–254.

45. Kurz, W., and D. J. Fisher. 1998. Fundamentals of Solidification. Trans Tech Publications, Zürich, Switzerland.